APPLICATIONS OF
MODELLING AND SIMULATION
http://arqiipubl.com/ams eISSN 2600-8084 VOL 10, 2026, 11-27

Optimal Brain Emotional Learning with PID Control for Flexible Joint Manipulators

Shahrizal Saat[1], Mohd Ashraf Ahmad[2,*], Mohd Zaidi Mohd Tumari[3], Mohd Helmi Suid[2] and Mohd Riduwan Ghazali[2]

[1]Faculty of Electronics and Computer Technology and Engineering, Universiti Teknikal Malaysia Melaka, Malaysia
[2]Faculty of Electrical and Electronics Engineering Technology, Universiti Malaysia Pahang Al-Sultan Abdullah, Malaysia
[3]Faculty of Electrical Technology and Engineering, Universiti Teknikal Malaysia Melaka, Malaysia

[*]Corresponding author: mashraf@umpsa.edu.my

Submitted 22 September 2025; Revised 21 October 2025; 03 November 2025; Available online 04 January 2026.

Abstract: This study introduces a data-driven Brain Emotional Learning-Based Intelligent Controller integrated with a Proportional-Integral-Derivative structure (BELBIC-PID) for a flexible joint manipulator (FJM) system. The controller is designed to enhance trajectory accuracy and dynamic performance in nonlinear plants where conventional PID controllers often exhibit shortcomings. To this end, the Modified Safe Experimentation Dynamics Algorithm (MSEDA) is employed to optimize the controller parameters, focusing on reducing tracking errors and minimizing input energy consumption. The nonlinear emotional learning process of the BELBIC further strengthens the controller's capability to manage complex system dynamics. The proposed BELBIC-PID is evaluated through fitness function minimization, time-domain analysis, and standard trajectory tracking indices. Two control schemes are implemented: one dedicated to angular position regulation and the other to link deflection suppression. The trajectory tracking results reveal that the BELBIC-PID achieves reductions of up to 26.56% in the Integral of Time multiplied Squared Error (ITSE), 37.55% in the Integral of Time multiplied Absolute Error (ITAE), 20.79% in the Integral of Squared Error (ISE), and 25.11% in the Integral of Absolute Error (IAE) compared with the PID controller for both system outputs, while also outperforming the Fractional-Order Proportional-Integral-Derivative (FOPID) and the Real Proportional-Integral-Derivative with Second-Order Derivative (RPIDD2) controllers. Furthermore, robustness evaluations under external disturbance and measurement noise conditions confirm that the BELBIC-PID maintains stable tracking performance and superior resilience. Overall, simulation outcomes demonstrate that the BELBIC-PID provides enhanced control accuracy and robustness for nonlinear systems.

Keywords: Brain emotional learning-based intelligent controller; Data-driven control; Flexible joint manipulators; Modified safe experimentation dynamics algorithm; Proportional-integral-derivative.

1. INTRODUCTION

Flexible joint manipulators (FJM) have become increasingly relevant in advanced robotic applications due to their lightweight design, energy efficiency, and suitability for high-speed motion. Previous studies have reported their successful use in diverse fields, including industrial automation [1], medical robotics [2], and space systems [3], where minimizing FJM oscillation and enhancing operational safety are essential considerations. Despite these advantages, the presence of joint flexibility gives rise to unwanted vibrations, nonlinear dynamics, and reduced positioning accuracy, which complicate motion control. These challenges highlight the need for effective control strategies that can maintain precise trajectory tracking and ensure robust performance under the influence of flexibility-induced uncertainties.

To address the challenges associated with joint flexibility, various model-based control strategies have been developed. Classical approaches such as computed torque control [4], feedback linearization [5], and Lyapunov stability-based control [6] rely on accurate dynamic models of the manipulator to achieve precise trajectory tracking. Advanced methods including robust H-infinity control [7], sliding mode control [8,9], backstepping control [10, 11], model predictive control [12], prescribed performance control [13], and boundary control [14, 15] have been applied to compensate for uncertainties, suppress vibrations, and enhance stability. Recently, reinforcement-learning-based and hybrid intelligent control approaches that combine neural and fuzzy learning mechanisms have been applied to manipulators, demonstrating adaptive capability and improved robustness under uncertain and nonlinear conditions [16-19]. Despite their effectiveness, these methods face several limitations. They require detailed knowledge of dynamic parameters, which may not be easily identifiable and can change during operation. The complex system dynamics and underactuation of FJM further complicate controller design, as the control input acts indirectly through the flexible joints rather than directly on the links. Consequently, maintaining accurate control

performance under modeling uncertainties and flexibility-induced nonlinearities remains a challenge.

As an alternative to model-based strategies, data-driven control approaches have gained increasing attention for their ability to regulate complex dynamics without requiring explicit knowledge of system parameters. These methods generate control actions directly from input-output measurements, while treating the plant as a black-box system. Such an assumption allows the effective handling of uncertainties and nonlinearities, making data-driven control particularly suitable for practical applications where precise modeling is difficult or impractical [20]. Additionally, advances in computational capabilities have enabled the use of optimization algorithms to tune controller parameters. Previous studies have widely applied PID controllers within data-driven control frameworks for FJM, using algorithms such as genetic algorithms [21], differential evolution [22], firefly algorithm [23], and particle swarm optimization [24, 25]. Moreover, the fractional-order PID (FOPID) controller extends the conventional PID formulation by introducing fractional differentiation and integration orders [26, 27]. In addition, the real PID with a second-order derivative (RPIDD2) represents an advanced variant designed to improve transient response and disturbance rejection [28, 29]. However, the linear characteristics of the PID and its variants restrict their effectiveness in handling the nonlinear dynamics and flexibility-induced vibrations of such systems, motivating the development of alternative controller structures. Therefore, fuzzy logic controllers have been investigated as an advanced method for improving trajectory tracking and reduce vibrations [30, 31]. Nevertheless, there remains a need for intelligent controller architectures that can further improve control accuracy and adaptability under complex and uncertain operating conditions.

This study introduces a brain-inspired control strategy for FJM to address the shortcomings of conventional PID controllers. The approach is motivated by the limbic system, which governs emotional learning and adaptive behavior in the human brain [32, 33]. Consequently, these learning mechanisms provide a foundation for developing intelligent control strategies capable of handling nonlinearities and uncertainties of the controlled system. The BELBIC is derived from a computational model of the limbic system, consisting of the thalamus, amygdala, orbitofrontal cortex, and sensory cortex [34]. Moreover, it operates based on two external stimuli: the sensory input (SI) and the reward signal (RW). The SI represents the system output relative to the reference, whereas the RW quantifies the effectiveness of the control action. The amygdala and orbitofrontal cortex process these signals, forming the emotional learning mechanism that governs the control action. In the proposed BELBIC-PID structure, the PID controller generates SI and RW, thereby providing structured input signals to guide emotional learning [35, 36]. Furthermore, combining the adaptive nonlinear learning of BELBIC with the simplicity of PID control is expected to enhance control accuracy, particularly in trajectory tracking and vibration suppression. Therefore, this integration introduces a novel approach to embedding a biologically inspired controller into data-driven control strategies for the FJM.

An advanced controller structure alone is insufficient without an effective parameter tuning algorithm, as inadequate tuning may prevent even sophisticated controllers from achieving optimal performance. Since the BELBIC-PID introduces more control parameters than the conventional PID, the choice of a tuning algorithm with low computational demand becomes particularly critical. In multi-agent optimization, the computational effort per iteration increases with the number of agents, which may lead to high computational cost when a large set of parameters is tuned [37]. By contrast, single-agent optimization techniques offer lower computational cost, making them attractive alternatives for such tasks. Several techniques, such as Simulated Annealing (SA) [38], Simultaneous Perturbation Stochastic Approximation (SPSA) [39], Stochastic Gradient Descent [41, 42], and Modified Safe Experimentation Dynamics Algorithm (MSEDA) [35] have been employed in data-driven control. Among these, the MSEDA [35] has been shown to be more effective because of its simple structure, memory-based updating rule, and a limited number of coefficients. Nevertheless, its application to BELBIC-PID control of FJM has not yet been explored. This study therefore aims to evaluate the BELBIC-PID tuned by MSEDA with the objective of enhancing control accuracy and minimizing oscillations in the tip response of the FJM.

This study develops a BELBIC-PID controller for the FJM, optimized using MSEDA in a data-driven framework. The external stimuli to the BELBIC, comprising the sensory input and the reward signal, are systematically generated from PID control in the proposed formulation. This approach combines the simplicity of PID with the adaptive emotional learning capability of BELBIC. The proposed structure is evaluated in terms of its ability to track trajectories and suppress manipulator vibrations. Two controllers are employed, one is responsible for regulating the tip angular position, while the other mitigates oscillations in the deflection angle. The evaluation includes the integral squared error of both outputs, the defined fitness function, and time-domain responses. Performance indices such as the Integral of Time multiplied Squared Error (ITSE), Integral of Time multiplied Absolute Error (ITAE), Integral of Squared Error (ISE), and Integral of Absolute Error (IAE) are also calculated to assess tracking accuracy. Simulation results confirm that the BELBIC-PID attains superior control performance compared with the conventional PID [40] and its advanced variants, FOPID [43] and RPIDD2 [44]. Based on these considerations, the key contributions of this study are summarized as follows:

(a) The sensory input and reward signal that stimulate the BELBIC emotional learning mechanism are structurally formulated based on the PID controller. This formulation, referred to as BELBIC-PID, represents the first implementation within a data-driven control framework for controlling a flexible joint manipulator (FJM).
(b) To obtain the optimal BELBIC-PID controller for the FJM, this study presents the initial implementation of the MSEDA, which effectively balances the exploration and exploitation phases during the control parameters tuning process.
(c) The control performance of the proposed BELBIC-PID is comprehensively evaluated and compared with benchmark controllers, including the conventional PID, FOPID, and RPIDD2.
(d) This work further evaluates the robustness of the proposed BELBIC-PID controller under external disturbance and measurement noise conditions, replicating realistic scenarios encountered in practical implementations.

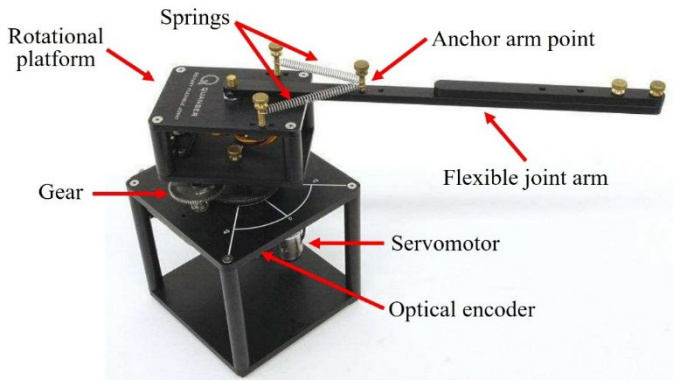

Figure 1. Overall structure of the FJM [31].

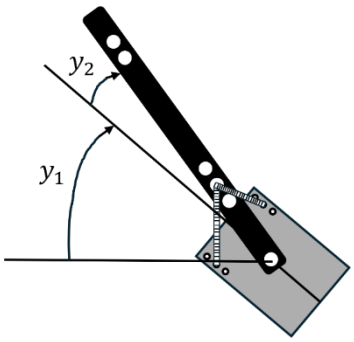

Figure 2. Illustration of tip and deflection angles in the FJM [31].

2. PROBLEM FORMULATION

In this section, the FJM system is described, and the BELBIC-PID control problem is formulated. It then outlines the procedure for tuning controller parameters using the MSEDA with the aim of minimizing a specified fitness function.

2.1 Flexible Joint Manipulator System

As depicted in Figure 1, the flexibility of the manipulator joint is modeled using a linear spring. The Quanser rotary joint module employs a high-gear servomotor to drive a lightweight arm coupled with two identical springs fixed on an aluminum frame [31]. Base rotation of the arm generates oscillations due to the elastic behavior of the springs. In Figure 2, y_1 denotes the tip angular displacement angle of the manipulator and y_2 represents the link deflection oscillation angle. The base motion, controlled by a servomotor, determines the tip angle position, while the spring compliance causes the link deflection oscillation according to its physical properties.

Furthermore, a brief model of the FJM is also introduced to establish the simulation environment for controller development. The system dynamics are derived using the Euler–Lagrange formulation to represent the nonlinear behavior of the manipulator. However, since the FJM is inherently nonlinear, a linearized model is adopted in this study for controller design and simulation. The linearization is performed around the equilibrium point under the assumptions of small angular deflections and low joint stiffness. These assumptions are widely adopted in FJM modeling to simplify the analysis while preserving the dominant system dynamics relevant to control design [39, 40]. The linearized dynamics of the FJM without control can be expressed in state–space form [31, 40] as

$$\dot{x} = Ax + Bu, y = Cx, \tag{1}$$

where the state vector is defined as

$$x = [y_1 \quad y_2 \quad \dot{y}_1 \quad \dot{y}_2]^T, \tag{2}$$

and the system matrices A, B, and C are given by

$$A = \begin{bmatrix} 0 & 0 & 1 & 0 \\ 0 & 0 & 0 & 1 \\ 0 & \frac{K_{stiff}}{J_{eq}} & \frac{-\eta_m\eta_g K_t K_m K_g^2 + B_{eq}R_m}{J_{eq}R_m} & 0 \\ 0 & \frac{-K_{stiff}(J_{eq}+J_{arm})}{J_{eq}J_{arm}} & \frac{\eta_m\eta_g K_t K_m K_g^2 + B_{eq}R_m}{J_{eq}R_m} & 0 \end{bmatrix}, B = \begin{bmatrix} 0 & 0 & \frac{\eta_m\eta_g K_t K_g}{J_{eq}R_m} & \frac{-\eta_m\eta_g K_t K_g}{J_{eq}R_m} \end{bmatrix}^T, \text{and } C = [1 \quad 0 \quad 0 \quad 0]. \tag{3}$$

In this formulation, the input u corresponds to the servomotor voltage V_m which governs the motion of the manipulator base. Moreover, the parameter values used in this model are summarized in Table 1.

Table 1. FJM configuration parameters [31, 40].

Symbol	Description	Value	Symbol	Description	Value
K_t	Motor torque constant (N.m/A)	0.00767	K_{stiff}	Joint stiffness (N.m/rad)	1.2485
R_m	Motor armature resistance (Ω)	2.60	K_g	Gear ratio	14:5
K_m	Motor voltage constant (V.s/rad)	0.00767	η_m	Efficiency of the motor	0.69
J_{eq}	Equivalent inertia (kg.m^2)	0.0026	η_g	Efficiency of the gear	0.90
J_{arm}	Arm link inertia (kg.m^2)	0.0035	B_{eq}	Damping coefficient (N.m.s/rad)	0.004

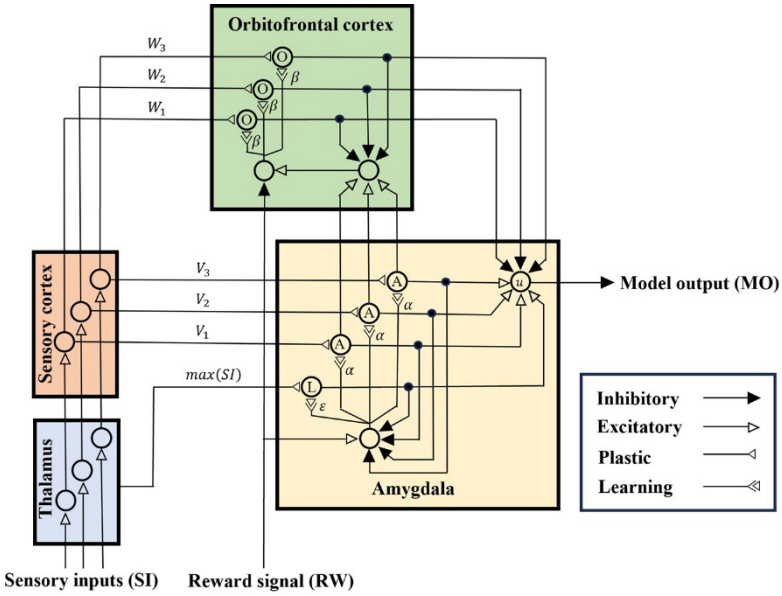

Figure 3. Structure of limbic system emotional learning [32].

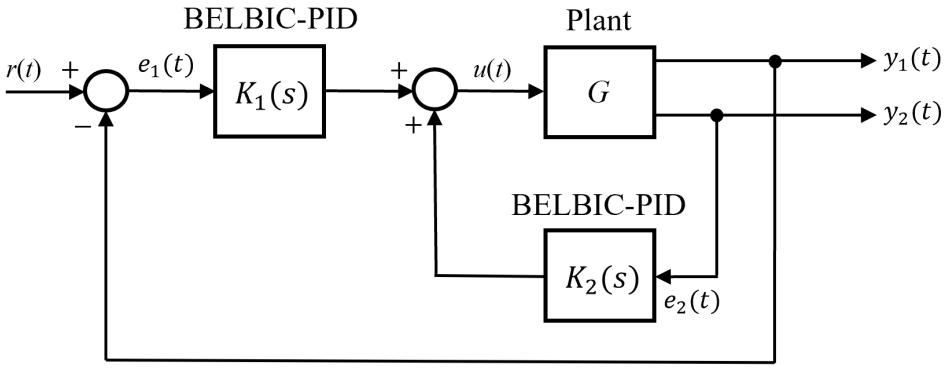

Figure 4. BELBIC-PID control system block diagram for FJM.

2.2 Formulation of the Data-Driven BELBIC-PID Problem

Figure 3 illustrates the structure of the emotional learning process in the limbic system [32], where the SI and RW signals in the proposed BELBIC are generated from the PID controller. It is noted that the structure of BELBIC is adopted from previous work [35, 45]. Figure 4 depicts the FJM system controlled by the BELBIC-PID. Next, the reference input for the desired tip position angle is denoted by $r(t)$, while the corresponding outputs are the tip angular position $y_1(t)$ and the deflection angle $y_2(t)$. The control input is represented by $u(t)$, and G denotes the FJM system. Additionally, two BELBIC-PID controllers, $K_1(s)$ and $K_2(s)$, are employed to process the error signals $e_1(t)$ and $e_2(t)$, which correspond to the tip angular position and deflection angle, respectively.

Furthermore, the BELBIC-PID controllers are formulated as

$$K_i(s) = B_i(M_i(s), N_i(s), SI_i(t), RW_i(t), l_i(t), a_i(t), o_i(t)) \tag{4}$$

for $i = 1, 2$, where i corresponds to the number of system outputs. Specifically, $i = 1$ corresponds to the tip angular position and $i = 2$ corresponds to the deflection oscillation angle. In this formulation, $M_i(s)$ and $N_i(s)$ represent the PID components for the sensory input and reward signal, respectively, while $SI_i(t)$ and $RW_i(t)$ denote the associated input signals. The terms $l_i(t)$, $a_i(t)$,and $o_i(t)$ correspond to the outputs of the thalamus, amygdala, and orbitofrontal cortex nodes, respectively.

Next, $M_i(s)$ and $N_i(s)$ are represented as PID controllers for the SI and RW, respectively, and are expressed as

$$M_i(s) = K_P^{SI}{}_i \left(1 + \frac{1}{K_I^{SI}{}_i s} + \frac{K_D^{SI}{}_i s}{1 + \left(\frac{K_D^{SI}{}_i}{N^{SI}{}_i}\right) s} \right), \tag{5}$$

and

$$N_i(s) = K_P^{RW}{}_i \left(1 + \frac{1}{K_I^{RW}{}_i s} + \frac{K_D^{RW}{}_i s}{1 + \left(\frac{K_D^{RW}{}_i}{N^{RW}{}_i}\right) s} \right). \tag{6}$$

Here, $K_P^{SI}{}_i \in \mathbb{R}$ denotes the proportional gain, $K_I^{SI}{}_i \in \mathbb{R}$ the integral time, $K_D^{SI}{}_i \in \mathbb{R}$ the derivative gain, and $N^{SI}{}_i \in \mathbb{R}$ the derivative filter coefficient, all associated with the SI. Similarly, $K_P^{RW}{}_i \in \mathbb{R}$, $K_I^{RW}{}_i \in \mathbb{R}$, $K_D^{RW}{}_i \in \mathbb{R}$, and $N^{RW}{}_i \in \mathbb{R}$ represent the corresponding parameters of the RW. By applying the inverse Laplace transform, the time-domain forms are given as $m_i(t) = \mathcal{L}^{-1}\{M_i(s)\}$ and $n_i(t) = \mathcal{L}^{-1}\{N_i(s)\}$. Accordingly, the output signals of SI and RW are defined as

$$SI_i(t) = m_i(t) \cdot e_i(t), \tag{7}$$

and

$$RW_i(t) = n_i(t) \cdot e_i(t), \tag{8}$$

where $e_i(t)$ denotes the error signal. For $i = 1$, the error signal is expressed as $e_1(t) = r(t) - y_1(t)$, representing the deviation between the desired and measured tip angular positions. For $i = 2$, the error signal is given by $e_2(t) = y_2(t)$, which directly corresponds to the deflection angle.

Subsequently, the SI and RW signals act on the emotional learning model of the limbic system, specifically affecting the thalamus, amygdala, and orbitofrontal cortex [45]. The thalamus node in the BELBIC-PID controller computes its output as

$$l_i(t) = (\max SI_i(t)) \cdot H_i(t), \tag{9}$$

where $l_i(t)$ denotes the thalamus node output and $H_i(t)$ is the plastic connection weight. The latter is updated according to

$$H_i(t) = \sum \Delta h_i(t) dt + H_i(0), \tag{10}$$

where $H_i(0)$ is the initial value of the weight. The weight update term $\Delta h_i(t)$ is expressed as

$$\Delta h_i(t) = \varepsilon_i \cdot SI_i(t) \cdot \max\left(0, RW_i(t) - l_i(t)\right), \tag{11}$$

with ε_i representing the emotional learning rate of the thalamus node. The thalamus acts as a sensory filter that forwards the maximum input signal to the amygdala for emotional processing [46].

Moreover, the response of the amygdala node is expressed as

$$a_i(t) = SI_i(t) \cdot V_{ij}(t), \tag{12}$$

The amygdala plastic connection, denoted by $V_i(t)$, is updated according to

$$V_i(t) = \sum \Delta v_i(t) dt + V_i(0), \tag{13}$$

where $V_i(0)$ is the initial value. The increment in the plastic weight, $\Delta v_i(t)$, is calculated as

$$\Delta v_i(t) = \alpha_i \cdot SI_i(t) \cdot \max(0, RW_i(t) - a_i(t) - l_i(t)), \tag{14}$$

with α_i denoting the emotional learning rate of the amygdala node. Accordingly, the amygdala processes the sensory input in conjunction with the reward signal to generate an adaptive control response. It functions as the principal learning mechanism by reinforcing control actions that minimize the error signal, thereby enhancing the regulation capability of the system [47].

Consequently, the output of the orbitofrontal cortex node is expressed as

$$o_i(t) = SI_i(t) \cdot W_i(t), \tag{15}$$

where $o_i(t)$ is the orbitofrontal cortex node output. The corresponding plastic connection, denoted by $W_i(t)$, is updated as

$$W_i(t) = \sum \Delta w_i(t) dt + W_i(0), \tag{16}$$

with $W_i(0)$ being the initial weight. The increment in the plastic weight, $\Delta w_i(t)$, is determined by

$$\Delta w_i(t) = \beta_i \cdot SI_i(t) \cdot \left(a_i(t) - o_i(t) - RW_i(t)\right), \tag{17}$$

where β_i represents the emotional learning rate of the orbitofrontal cortex node. Consequently, the orbitofrontal cortex provides a corrective learning mechanism by suppressing unsuitable responses generated by the amygdala. It refines the control signal by incorporating feedback from past outcomes, thereby ensuring balanced regulation of the system [48].

Finally, the BELBIC-PID controllers $B_i(M_i(s), N_i(s), SI_i(t), RW_i(t), l_i(t), a_i(t), o_i(t))$ are implemented for the flexible joint manipulator shown Figure 4, and is computed as

$$u(t) = \sum_{i=1}^{2} a_i - o_i. \tag{18}$$

In this structure, BELBIC-PID output is computed as the difference between the amygdala response, which drives the control action, and the orbitofrontal cortex response, which regulates it to avoid excessive control effort [49].

The aim is to construct a data-driven BELBIC-PID controller that ensures the tip angle follows the reference trajectory with minimal oscillatory deflection. Accordingly, the control fitness function in Equation (19) is defined as:

$$J(\boldsymbol{K_P^{SI}}, \boldsymbol{K_I^{SI}}, \boldsymbol{K_D^{SI}}, \boldsymbol{N^{SI}}, \boldsymbol{K_P^{RW}}, \boldsymbol{K_I^{RW}}, \boldsymbol{K_D^{RW}}, \boldsymbol{N^{RW}}, \boldsymbol{\varepsilon}, \boldsymbol{\alpha}, \boldsymbol{\beta}) = w_1\hat{y}_1 + w_2\hat{y}_2 + w_3\hat{u}, \tag{19}$$

with

$$\hat{y}_1 = \int_{t_0}^{t_f} |r(t) - y_1(t)|^2 dt, \tag{20}$$

$$\hat{y}_2 = \int_{t_0}^{t_f} |y_2(t)|^2 dt, \tag{21}$$

$$\hat{u} = \int_{t_0}^{t_f} |u(t)|^2 dt, \tag{22}$$

The coefficient w_1, w_2 and $w_3 \in \mathbb{R}$ serve as weights that regulate the fitness function. In Equation (19), the tuning parameters are defined as $\boldsymbol{K_P^{SI}} = [K_{P\,1}^{SI} \quad K_{P\,2}^{SI}]^T$, $\boldsymbol{K_I^{SI}} = [K_{I\,1}^{SI} \quad K_{I\,2}^{SI}]^T$, $\boldsymbol{K_D^{SI}} = [K_{D\,1}^{SI} \quad K_{D\,2}^{SI}]^T$, $\boldsymbol{N^{SI}} = [N_1^{SI} \quad N_2^{SI}]^T$, $\boldsymbol{K_P^{RW}} = [K_{P\,1}^{RW} \quad K_{P\,2}^{RW}]^T$, $\boldsymbol{K_I^{RW}} = [K_{I\,1}^{RW} \quad K_{I\,2}^{RW}]^T$, $\boldsymbol{K_D^{RW}} = [K_{D\,1}^{RW} \quad K_{D\,2}^{RW}]^T$, $\boldsymbol{N^{RW}} = [N_1^{RW} \quad N_2^{RW}]^T$, $\boldsymbol{\varepsilon} = [\varepsilon_1 \quad \varepsilon_2]$, $\boldsymbol{\alpha} = [\alpha_1 \quad \alpha_2]$, and $\boldsymbol{\beta} = [\beta_1 \quad \beta_2]$. These parameters together constitute 22 variables in the BELBIC-PID controller. The evaluation period is considered within the interval $[t_0, t_f]$, where the initial time t_0 belong to $\{0\} \cup \mathbb{R}_+$ and the final time t_f is in $\mathbb{R}_+$. Finally, the controller design problem can be stated as follows:

Problem 1: For the plant *G* with the BELBIC-PID structure in Figure 4 and given input–output data, determine the controller parameters $K_1(s)$ and $K_2(s)$ that minimize the fitness function in Equation (19).

2.3 Data-driven BELBIC-PID Based on Modified Safe Experimentation Dynamics Algorithm

This section outlines the formulation of the BELBIC-PID for the FJM, optimized using the MSEDA. For completeness, a brief overview of the original SEDA [50] is first provided, followed by a description of its improved variant, the MSEDA [35]. The section concludes by detailing the procedure for tuning the BELBIC-PID controller using MSEDA.

To minimize the fitness function defined in Equation (19), the optimization problem is formulated as:

$$\min_{\boldsymbol{x}(k) \in \mathbb{R}^n} f(\boldsymbol{x}(k)) \tag{23}$$

where $f: \mathbb{R}^n \to \mathbb{R}$ and $\boldsymbol{x}(k) \in \mathbb{R}^n$ denotes the fitness function and the design parameters at the k-th iteration, respectively. The objective as stated in Problem 1 is to update the design parameters until the maximum iteration k_{max} is reached to determine the optimal solution $\boldsymbol{x}_{opt} \in \mathbb{R}^n$. The update rule of SEDA is given by:

$$x_i(k+1) = \begin{cases} h(\gamma) & \text{, if } rv_1 < E, \\ \bar{x}_i & \text{, if } rv_1 \geq E, \end{cases} \tag{24}$$

with

$$\gamma = (\bar{x}_i - K_g \cdot rv_2), \tag{25}$$

where, x_i is the design vector $\boldsymbol{x}$, and $\bar{x}_i$ is the current best solution $\bar{\boldsymbol{x}}$, for the i-th element. The scalar K_g denotes the step interval for random perturbations, while E specifies the probability of updating the parameter. The random variable rv_1 is uniformly distributed in the range [0,1], and rv_2 is selected within the bounds $[x_{min}, x_{max}]$. The candidate solution function $h(\gamma)$ is defined as:

$$h(\gamma) = \begin{cases} x_{max}, & \gamma > x_{max}, \\ \gamma, & x_{min} \leq \gamma \leq x_{max}, \\ x_{\min}, & \gamma < x_{min}. \end{cases} \tag{26}$$

The step-by-step procedure of the SEDA is summarized as follows:
S1: Set the lower and upper bounds x_{min} and x_{max}, define K_g and E, then initialize the vector $\boldsymbol{x}(0)$. Evaluate its fitness function $f(\boldsymbol{x}(0))$ and record it as $\bar{\boldsymbol{x}} = \boldsymbol{x}(0)$ with $\bar{f} = f(\boldsymbol{x}(0))$.
S2: If $f(\boldsymbol{x}(k)) < \bar{f}$, update the best solution as $\bar{\boldsymbol{x}} = \boldsymbol{x}(k)$ and $\bar{f} = f(\boldsymbol{x}(k))$. If not, proceed to **S3**.
S3: Two independent random numbers, rv_1 and rv_2, are generated, and the update rule in Equation (24) is applied to form a new candidate solution.
S4: Compute the fitness function value for the updated solution, $f(\boldsymbol{x}(k+1))$.
S5: Check whether the stopping criterion is satisfied, typically the iteration limit k_{max}, stop the algorithm and return the optimal tuning vector $\boldsymbol{x}_{opt} \coloneqq \underset{\boldsymbol{x}\in\{\boldsymbol{x}(0),\boldsymbol{x}(1),\ldots,\boldsymbol{x}(k+1)\}}{\arg\min} f(\boldsymbol{x})$.

In the standard SEDA, the update rule in Equation (24) is controlled by the constant probability coefficient E. This formulation restricts the algorithm by disallowing any adjustment to the exploration–exploitation balance during iterations. Conceptually, exploration and exploitation are contrasting objectives, such that strengthening one generally weakens the performance of the other. Therefore, a dynamic probability coefficient is proposed to overcome this limitation as follows:

$$E(k) = 1 - \lambda, \tag{27}$$

with $\lambda = \left(\frac{K_e \cdot k}{k_{max}}\right)$. As the iterations proceed, $E(k)$ converges progressively due to λ, which is an iteration-dependent scaling factor that increases with k. The parameter K_e is a predefined constant less than one, and it determines the rate of reduction. Incorporating this dynamic probability into the update law, the modified SEDA update equation is formulated as:

$$x_i(k+1) = \begin{cases} h(\gamma), & \text{if } rv_1 < E(k), \\ \bar{x}_i \quad , & \text{if } rv_1 \geq E(k), \end{cases} \tag{28}$$

where the update decision now adapts according to the iteration-dependent probability coefficient.

Therefore, with the introduction of the linear decreasing probability coefficient in Equation (27), the algorithm is expected to enhance coordination between exploration and exploitation. At early iterations (small k), the probability $E(k)$ is high, resulting in frequent perturbations of the design parameters. During this phase, the search space is extensively explored, which minimizes the likelihood of convergence to a local optimum. Conversely, toward the later stages (large k), the probability $E(k)$ decreases, resulting in fewer perturbations. At this stage, the algorithm emphasizes intensification around promising regions of the solution space to refine the search for the global optimum.

Accordingly, using the update rule provided in Equation (28), the method for implementing MSEDA to optimize the BELBIC-PID controller for the FJM is outlined below:
P1: Define the maximum iteration k_{max} and set the fitness function $f(\boldsymbol{x}) = J(\boldsymbol{K_P^{SI}}, \boldsymbol{K_I^{SI}}, \boldsymbol{K_D^{SI}}, \boldsymbol{N^{SI}}, \boldsymbol{K_P^{RW}}, \boldsymbol{K_I^{RW}}, \boldsymbol{K_D^{RW}}, \boldsymbol{N^{RW}}, \boldsymbol{\varepsilon}, \boldsymbol{\alpha}, \boldsymbol{\beta})$ with $x_i = log\, \psi_i$. The tuning vector is $\psi = [K_{P\,1}^{SI}\ K_{I\,1}^{SI}\ K_{D\,1}^{SI}\ N_1^{SI}\ K_{P\,1}^{RW}\ K_{I\,1}^{RW}\ K_{D\,1}^{RW}\ N_1^{RW}\ \varepsilon_1\ \alpha_1\ \beta_1\ K_{P\,2}^{SI}\ K_{I\,2}^{SI}\ K_{D\,2}^{SI}\ N_2^{SI}\ K_{P\,2}^{RW}\ K_{I\,2}^{RW}\ K_{D\,2}^{RW}\ N_2^{RW}\ \varepsilon_2\ \alpha_2\ \beta_2]^T$, and $\psi_i = 10^{x_i}$ for $i = 1,2,\ldots,22$. To expedite the optimization process, the design parameters are expressed on a logarithmic scale.
P2: Execute the MSEDA algorithm.
P3: After reaching k_{max}, obtain the optimal solution $\boldsymbol{x}_{opt} = \bar{\boldsymbol{x}}$. Then, the system shown in Figure 4 is controlled using the optimal BELBIC-PID parameters, given by $\psi_{opt} = [10^{\bar{x}_1} \quad 10^{\bar{x}_2} \quad \cdots \quad 10^{\bar{x}_{22}}]^T$.

Remark 2.3: This study was conducted entirely through simulation using a plant model that has been validated in previous studies [31]. The proposed method is based on a data-driven control framework, where the controller parameters are determined directly from the measured input–output data without relying on an explicit plant model. From this perspective, analytical verification of closed-loop stability is not feasible. Therefore, stability in this work is examined by confirming that the system output remains bounded and converges to a steady-state without divergence during the simulation period.

3. RESULTS AND ANALYSIS

This section evaluates the performance of the FJM system controlled by the proposed BELBIC-PID, with comparison against the conventional PID [40], FOPID [43] and RPIDD2 [44]. The evaluation is based on the following criteria:

(a) The fitness function value, including the total ISE and ISI, as defined in Equations (19) – (22).
(b) The transient response of the tip angular position $y_1(t)$ and the deflection angle $y_2(t)$, with focus on maximum overshoot (M_p), settling time (T_s), and steady-state error (E_{ss}).
(c) The robustness evaluation of all controllers under external disturbance and measurement noise conditions to examine their control accuracy and adaptability in realistic operating environments.
(d) The trajectory tracking performance for both $y_1(t)$ and $y_2(t)$, assessed using four integral error indices: IAE, ISE, ITAE, and ITSE. These indices are defined as:

$$\text{IAE} = \int_0^{t_f} |e_i(t)|dt, \tag{29}$$

$$\text{ISE} = \int_0^{t_f} e_i^2(t)dt, \tag{30}$$

$$\text{ITAE} = \int_0^{t_f} t|e_i(t)|dt, \tag{31}$$

$$\text{ITSE} = \int_0^{t_f} te_i^2(t)dt, \tag{32}$$

where t_f denotes the final simulation time set to 4 seconds, and $e_i(t)$ represents the error signal. For $i = 1$, the error signal is expressed as $e_1(t) = r(t) - y_1(t)$, while for $i = 2$, the error signal is given by $e_2(t) = y_2(t)$.

In this study, flexible joint plant model *G* adopted in this work follows the formulation presented in [31,40]. For the time interval $0 < t < 4$ seconds, the reference trajectory $r(t)$ is defined as:

$$r(t) = 25\big(\tanh\big(0.005(t - 0.7)\big) + 1\big). \tag{33}$$

This study aims to design an optimal BELBIC-PID controller to achieve precise tracking of the tip angular position according to Equation (33) while reducing oscillatory deflection. The MSEDA algorithm coefficients are selected as $K_g = 0.022$, $K_e = 0.75$, $x_{min} = -5$, and $x_{max} = 5$. The weighting factors are chosen as $w_1 = 400$, $w_2 = 200$ and $w_3 = 2$. To allow a fair comparison with the benchmark controllers, the simulation time and weighting factors are kept identical to those reported in [40]. Consequently, the maximum number of iterations is set to $k_{max} = 2000$ to ensure convergence toward optimal performance.

Furthermore, to establish the initial design vector $10^{x(0)} \in \mathbb{R}^{22}$, several preliminary trials were conducted to ensure bounded system output throughout the simulation. Tables 2, 3, and 4 present the optimal control parameters for the PID, FOPID, and RPIDD2 controllers, respectively, while Table 5 summarizes the finalized initial parameters together with the optimized BELBIC-PID control parameters. It should be noted that the benchmark PID controller was optimized using the Adaptive Safe Experimentation Dynamics Algorithm (ASEDA), while the FOPID and RPIDD2 controllers were optimized using MSEDA. The convergence of the fitness function $J(\boldsymbol{\psi})$ throughout the optimization process for all controllers is illustrated in Figures 5(a)-(d), corresponding to PID-ASEDA, FOPID-MSEDA, RPIDD2-MSEDA, and BELBIC-PID-MSEDA, respectively. As shown in Figures 5(a)-(d), the fitness function of the proposed BELBIC-PID controller approaches saturation at approximately 1200 iterations, while the benchmark controllers reach their saturation conditions much earlier, around 150 iterations. This behavior corresponds to the higher number of control parameters in the proposed BELBIC-PID controller compared with the benchmark controllers. Additionally, the system responses for the tip angular position $y_1(t)$ and the deflection angle $y_2(t)$ obtained from all controllers are illustrated in Figures 6 and 7, respectively, with their close up views provided in Figures 8 and 9. Consequently, the corresponding control inputs generated by each controller are depicted in Figure 10, and their magnified views are presented in Figure 11. The results demonstrate that the BELBIC-PID outperformed the PID, FOPID, and RPIDD2 controllers in trajectory tracking, achieving reductions of 15.32%, 14.29%, and 9.48%, respectively, in the fitness function $J(\boldsymbol{\psi})$. Moreover, this improvement is further supported by lower total integral squared error and integral squared input values, as reported in Table 6, where the bold entries highlight the best performance. The FOPID and RPIDD2 controllers achieve reductions of 2.73% and 8.10% in control input energy compared with the PID controller, but at the expense of higher trajectory tracking error. In contrast, the proposed BELBIC-PID strikes a balance between tracking accuracy and control efficiency, delivering the lowest tracking error with minimal control effort and consistently outperforming the benchmark controllers.

Table 2. Optimal design parameters of the PID-ASEDA controller [40].

Controller	K_{p1}	K_{i1}	K_{d1}	N_1	K_{p2}	K_{i2}	K_{d2}	N_2
PID	20.8593	8.0316	0.5550	163.9834	0.2035	13.0227	0.3278	66.9576

Table 3. Optimal design parameters of the FOPID-MSEDA controller [43].

Controller	K_{p1}	K_{i1}	K_{d1}	λ_1	μ_1
FOPID	19.1231	25.1049	13.3885	0.3391	1.0161
	K_{p2}	K_{i2}	K_{d2}	λ_2	μ_2
	1.6021	36.2433	0.2999	0.3877	0.1128

Table 4. Optimal design parameters of the RPIDD2-MSEDA controller [44].

Controller	K_{p1}	K_{i1}	K_{d1}	N_{11}	K_{dd1}	N_{12}	N_{13}
RPIDD2	24.4411	1.0505	10.5518	11.5699	0.9515	54.1393	61.8822
	K_{p2}	K_{i2}	K_{d2}	N_{21}	K_{dd2}	N_{22}	N_{23}
	0.5981	2.2015	1.7011	4.0323	0.0866	2.9774	4.9265

Table 5. BELBIC-PID-MSEDA optimal design parameters.

$\boldsymbol{\psi}$	BELBIC-PID parameters	$\boldsymbol{x}(0)$	$10^{\boldsymbol{x}(0)}$	$\boldsymbol{x}_{opt}$	$10^{\boldsymbol{x}_{opt}}$
ψ_1	$K_{P\ 1}^{SI}$	1.00	10.0000	0.12	1.3035
ψ_2	$K_{I\ 1}^{SI}$	1.00	10.0000	1.10	12.4693
ψ_3	$K_{D\ 1}^{SI}$	0.00	1.0000	-0.38	0.4215
ψ_4	N_{1}^{SI}	2.00	1×10^2	2.52	3.3190×10^2
ψ_5	$K_{P\ 1}^{RW}$	1.00	10.0000	2.61	4.0799×10^2
ψ_6	$K_{I\ 1}^{RW}$	1.00	10.0000	0.24	1.7221
ψ_7	$K_{D\ 1}^{RW}$	0.00	1.0000	1.64	43.1969
ψ_8	N_{1}^{RW}	2.00	1×10^2	0.29	1.9520
ψ_9	ε_1	-3.00	0.0010	-3.57	0.0003
ψ_{10}	α_1	0.50	3.1623	1.00	10.0713
ψ_{11}	β_1	-3.00	0.0010	-3.12	0.0008
ψ_{12}	$K_{P\ 2}^{SI}$	-0.50	0.3162	-0.96	0.1094
ψ_{13}	$K_{I\ 2}^{SI}$	1.00	10.0000	1.78	60.5438
ψ_{14}	$K_{D\ 2}^{SI}$	-0.50	0.3162	-0.27	0.5353
ψ_{15}	N_{2}^{SI}	2.00	1×10^2	2.26	1.8222×10^2
ψ_{16}	$K_{P\ 2}^{RW}$	-0.50	0.3162	-1.16	0.0698
ψ_{17}	$K_{I\ 2}^{RW}$	1.00	10.0000	1.14	13.9213
ψ_{18}	$K_{D\ 2}^{RW}$	-0.50	0.3162	-1.17	0.0671
ψ_{19}	N_{2}^{RW}	2.00	1×10^2	1.31	20.2840
ψ_{20}	ε_2	-3.00	0.0010	-3.39	0.0004
ψ_{21}	α_2	0.50	3.1623	1.35	22.5334
ψ_{22}	β_2	-3.00	0.0010	-2.13	0.0074

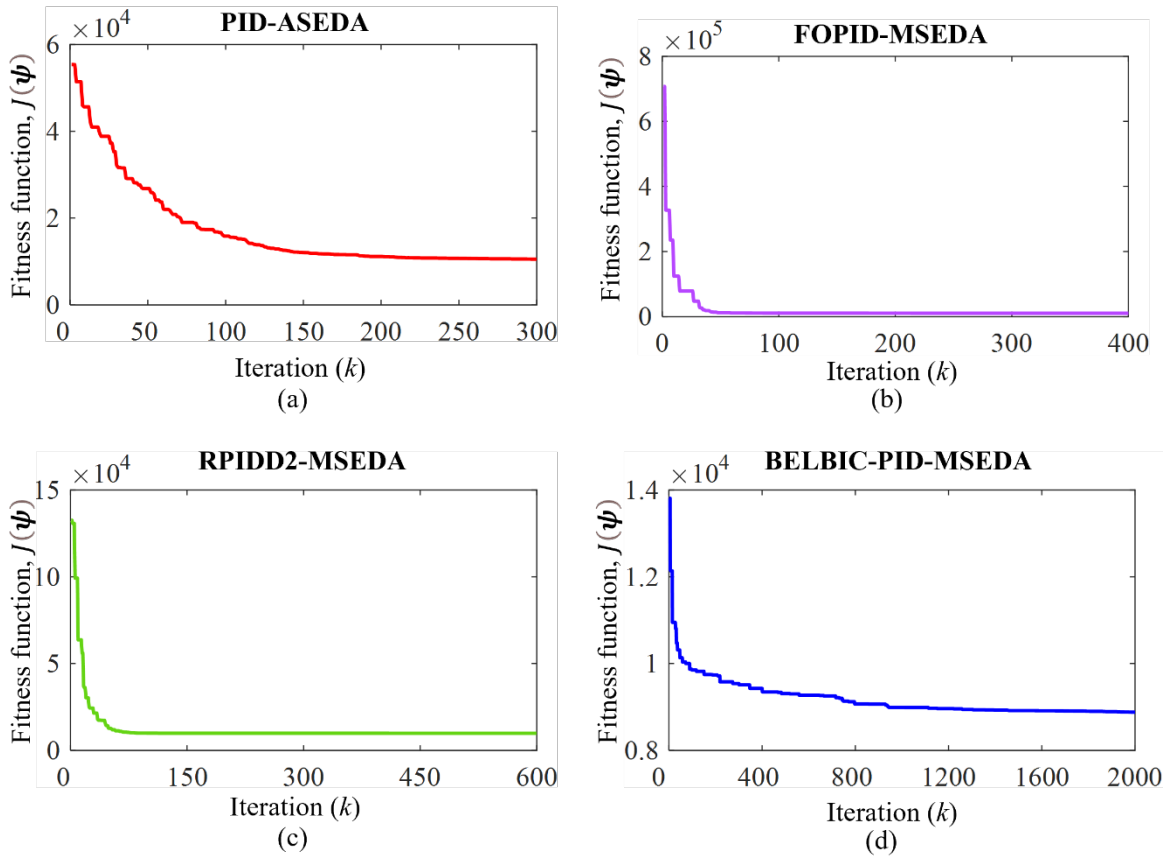

Figures 5. Convergence curve of the fitness function $J(\boldsymbol{\psi})$ for (a) PID-ASEDA, (b) FOPID-MSEDA, (c) RPIDD2-MSEDA, and (d) BELBIC-PID-MSEDA controllers.

Table 6. Numerical results of the FJM controllers.

Controller	PID [40]	FOPID [43]	RPIDD2 [44]	BELBIC-PID
Fitness function, $J(\boldsymbol{\psi})$ $(\times 10^3)$	10.4879	10.3620	9.8101	**8.8803**
Total ISE, $\sum_{j=1}^{2} \bar{e}_j$	3.3680	3.6225	3.4846	**2.7470**
ISI, $\bar{u}$ $(\times 10^3)$	4.7826	4.6519	4.3950	**4.0588**

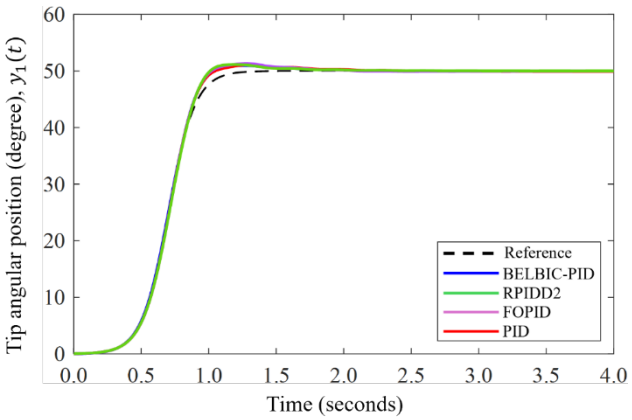

Figure 6. Tip angular position responses.

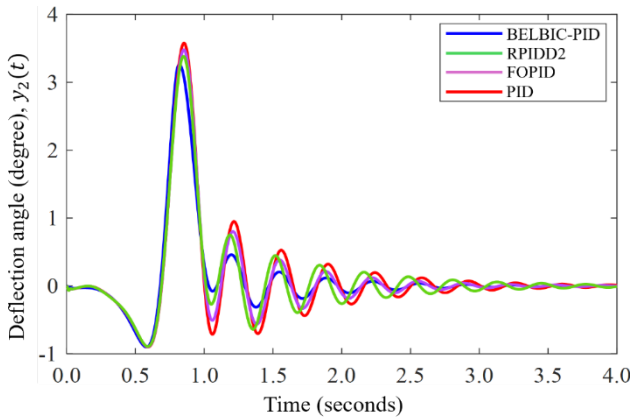

Figure 7. Deflection angle responses.

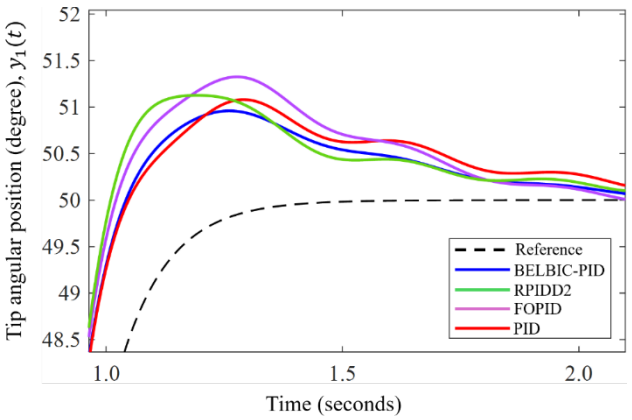

Figure 8. Zoomed view of the tip angular position responses.

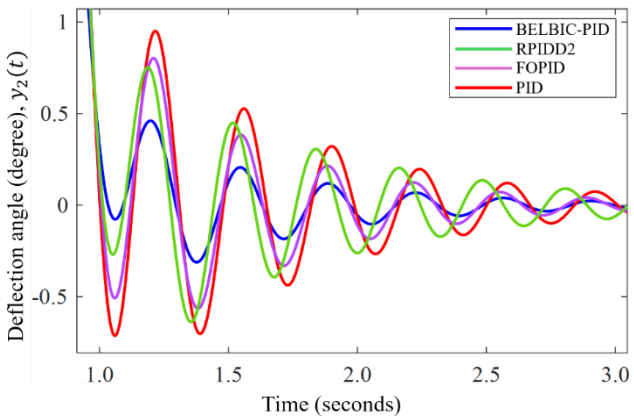

Figure 9. Zoomed view of the deflection angle responses.

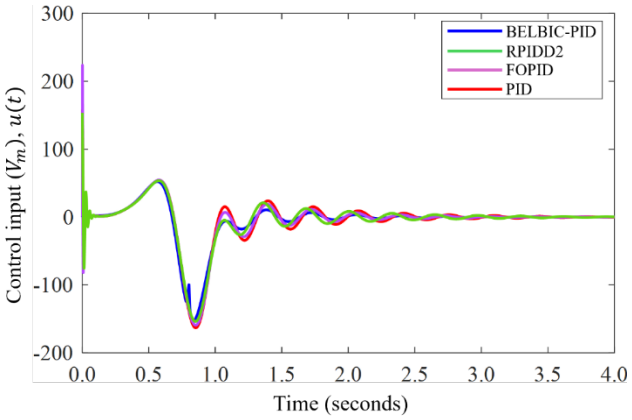

Figure 10. Control input responses.

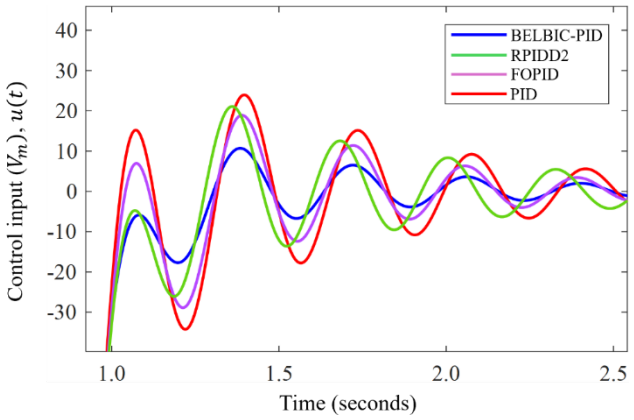

Figure 11. Zoomed view of the control input responses.

Additionally, Table 7 presents a comparison of the time-response performance of the PID, FOPID, RPIDD2, and the proposed BELBIC-PID controllers for the outputs $y_1(t)$ and $y_2(t)$. The benchmark PID controller shows clear limitations in handling the nonlinear dynamics of the FJM, producing a prolonged settling time of 3.7970 seconds and a maximum peak of 3.57% in the deflection angle response $y_2(t)$. The FOPID controller improves the settling time to 3.2530 seconds, while RPIDD2 reduces the maximum peak to 3.38%. In contrast, the BELBIC-PID controller yields the lowest values for all performance measures in the deflection angle response $y_2(t)$ relative to the benchmark controllers. For the tip angular position $y_1(t)$, the BELBIC-PID controller achieves lower values for all time-response metrics compared with the PID controller. In addition, the proposed BELBIC-PID shows comparable results to FOPID and RPIDD2 in terms of steady-state error, while yielding the fastest settling time and smallest maximum peak value. To further evaluate the controller's performance, four integral error indices were considered: ITSE, ITAE, ISE, and IAE, as summarized in Table 8. The results indicate that the BELBIC-PID controller consistently achieves the lowest value across all indices for $y_1(t)$ and $y_2(t)$. These results confirm that the nonlinear structure of the BELBIC-PID enhances control accuracy and improves the overall dynamic performance of the system compared with the PID controller and its advanced variants.

Table 7. Time response analysis results of the FJM controllers.

Responses measured	Time response metrics	PID [40]	FOPID [43]	RPIDD2 [44]	BELBIC-PID
Tip angular position (degree), $y_1(t)$	Maximum peak, M_P	51.0804	51.3247	51.1261	**50.9594**
	Settling time (2%), $T_s(s)$	1.3460	1.3990	1.3020	**0.9890**
	Steady state error, E_{ss}	0.0878	0.0138	**0.0028**	0.0610
Deflection angle (degree), $y_2(t)$	Maximum peak, M_P	3.5772	3.4775	3.3818	**3.2581**
	Settling time (2%), $T_s(s)$	3.7970	3.2530	3.8110	**2.9330**
	Steady state error, E_{ss}	0.0084	0.0021	0.0068	**0.0009**

Table 8. Trajectory tracking of the BELBIC-PID and benchmark controllers.

Responses measured	Performance indices	PID [40]	FOPID [43]	RPIDD2 [44]	BELBIC-PID
Tip angular position (degree), $y_1(t)$	ITSE	1.4093	1.8543	1.7204	**1.2073**
	ITAE	1.8554	1.7890	1.5926	**1.4984**
	ISE	1.2461	1.6694	1.6163	**1.0664**
	IAE	1.3955	1.4632	1.3758	**1.1264**
Deflection angle (degree), $y_2(t)$	ITSE	1.8851	1.6874	1.6315	**1.3841**
	ITAE	1.5101	1.2316	1.3724	**0.9425**
	ISE	2.1219	1.9531	1.8683	**1.6806**
	IAE	1.3672	1.2124	1.2499	**1.0237**

3.1 Robustness Evaluation of BELBIC-PID Under External Disturbance

Evaluating the controller capability to withstand external disturbances is essential for assessing its robustness. Therefore, the proposed BELBIC-PID controller was evaluated together with the benchmark controllers under disturbance conditions. The simulation setup was identical to the trajectory tracking experiment, except that an additional disturbance signal $D(t)$ was applied to the deflection angle output $y_2(t)$, as illustrated in Figure 12. The corresponding disturbance signal is shown in Figure 13 and defined as:

$$D(t) = \begin{cases} 2, & \text{for} \quad 0.6 \leq t \leq 0.8, \\ -2, & \text{for} \quad 2.0 \leq t \leq 2.2, \\ 0, & elsewhere. \end{cases} \tag{34}$$

As described in Equation (34), the disturbance signal $D(t)$ represents abrupt variations in the deflection angle that emulate real operating conditions. Each disturbance lasted for 0.2 seconds with an amplitude of not less than $\pm$50% relative to the maximum deflection angle during optimal trajectory tracking. The disturbance signals was applied alternately in both positive and negative directions of the deflection angle to represent bidirectional oscillations. All controller parameters used in this evaluation were identical to those listed in Tables 2-5.

Furthermore, the system responses for the tip angular position $y_1(t)$ and deflection angle $y_2(t)$ obtained from all controllers under external disturbance are illustrated in Figures 14 and 15, respectively, with their close up views shown in Figures 16 and 17. It can be observed that the BELBIC-PID exhibits minimal output deviation and rapid recovery following each disturbance, confirming its superior disturbance rejection capability, particularly for the deflection angle $y_2(t)$. The PID, FOPID, and RPIDD2 controllers produced similar responses characterized by larger oscillation amplitudes and longer recovery times, whereas the BELBIC-PID exhibited lower sensitivity to the disturbance throughout the disturbance intervals. Consequently, the corresponding control inputs generated by each controller to compensate for the disturbance signal are depicted in Figure 18. The BELBIC-PID produced a more responsive and well coordinated control action, demonstrating better adaptability and reduced sensitivity to external perturbations.

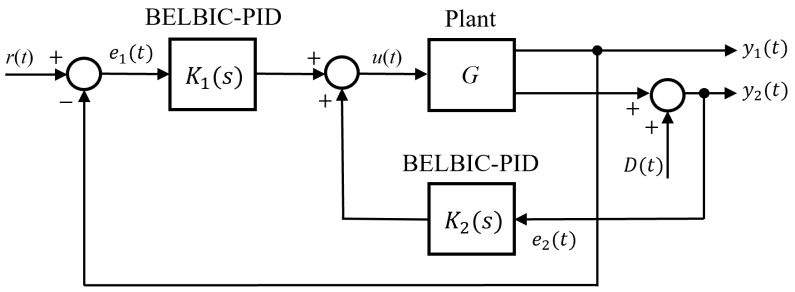

Figure 12. Deflection angle response of the FJM under external disturbance.

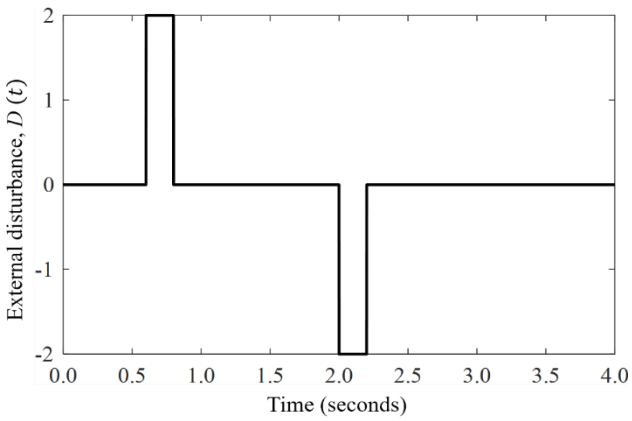

Figure 13. An additional disturbance signal, $D(t)$.

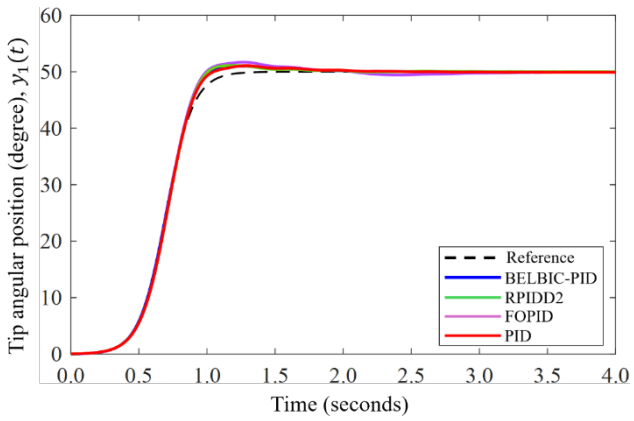

Figure 14. Tip angular position responses under external disturbance.

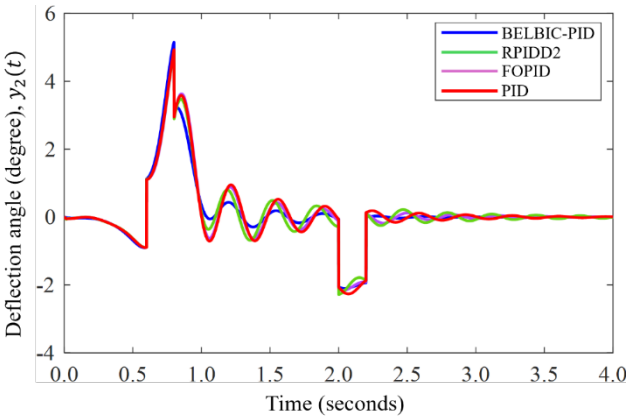

Figure 15. Deflection angle responses under external disturbance.

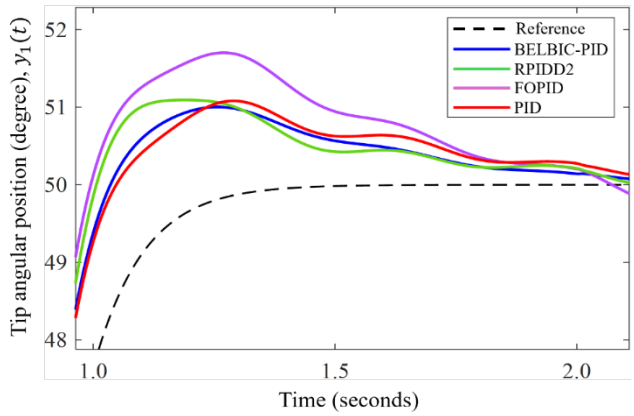

Figure 16. Zoomed view of the tip angular position responses under external disturbance.

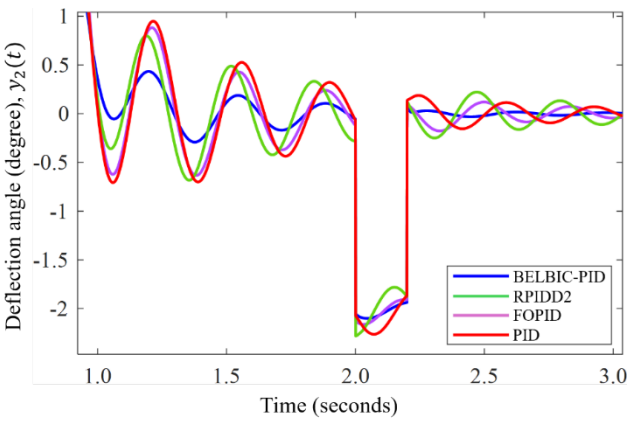

Figure 17. Zoomed view of the deflection angle responses under external disturbance.

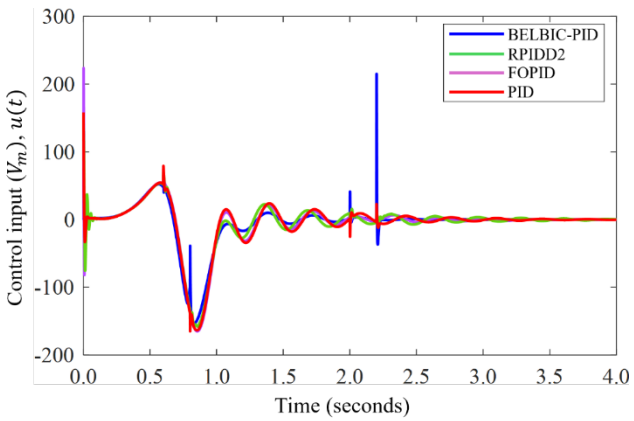

Figure 18. Control input responses under external disturbance.

Table 9. Trajectory tracking of the BELBIC-PID and benchmark controllers under external disturbance.

Responses measured	Performance indices	PID [40]	FOPID [43]	RPIDD2 [44]	BELBIC-PID
Tip angular position (degree), $y_1(t)$	ITSE	1.4079	3.4201	1.7594	**1.3209**
	ITAE	1.8486	3.2236	1.6504	**1.5698**
	ISE	1.2445	2.8200	1.6526	**1.1662**
	IAE	1.3913	2.1809	1.3936	**1.1783**
Deflection angle (degree), $y_2(t)$	ITSE	4.6872	4.4727	4.2629	**4.1510**
	ITAE	2.5364	2.3765	2.5017	**1.9464**
	ISE	4.2478	4.1303	3.9540	**3.8991**
	IAE	2.0490	1.9642	1.9820	**1.7076**

Moreover, Table 9 summarizes the performance indices of the BELBIC-PID and benchmark controllers under external disturbance conditions. For the tip angular position response $y_1(t)$, the BELBIC-PID achieved the lowest values across all error based indices, specifically ITSE, ITAE, ISE, and IAE, with respective reductions of 6.18%, 15.08%, 6.29%, and 15.31% compared with the PID controller. These results show that the proposed controller effectively reduces tracking errors and improves transient behavior during disturbance conditions. For the deflection angle response $y_2(t)$, the BELBIC-PID consistently yielded the lowest ITAE and IAE values of 1.9464 and 1.7076, while maintaining small ITSE and ISE values relative to the benchmark controllers. In comparison with the PID, FOPID, and RPIDD2 controllers, the BELBIC-PID reduced ITAE by 23.26%, 18.09%, and 22.19%, respectively, and lowered IAE by 16.67%, 13.06%, and 13.84%, demonstrating clear improvements in vibration suppression. The superior robustness of the BELBIC-PID is attributed to its emotional learning mechanism, which adaptively adjusts the control signal to counteract disturbance effects and sustain stable operation.

3.2 Robustness Evaluation of BELBIC-PID Under Measurement Noise

To further examine the controllers robustness under realistic operating conditions, a trajectory tracking simulation was conducted with the presence of measurement noise $d_{noise}(t)$. In this test, the noise was modeled as zero mean white noise with a variance of 0.1. This noise model represents a sufficiently strong disturbance signal to evaluate the sensitivity and robustness of each controller under noisy feedback conditions. The overall configuration of the robustness test, in which measurement noise is applied to $y_2(t)$, is illustrated in Figure 19. In this setup, the measured signal $\hat{e}_2(t)$ is obtained by summing the actual deflection signal $e_2(t)$ with the measurement noise signal $d_{noise}(t)$. The corresponding white noise signal used in this test is depicted in Figure 20. All controller parameters employed in this evaluation are identical to those listed in Tables 2–5.

Under measurement noise conditions, the system exhibits noticeable variations in tracking behavior among the evaluated controllers. Figures 21 and 22 illustrate the responses of the tip angular position $y_1(t)$ and the deflection angle $y_2(t)$, while Figures 23 and 24 provide magnified sections for closer inspection. Despite the introduction of the measurement noise signal $d_{noise}(t)$ into the measured deflection angle $e_2(t)$, the BELBIC-PID maintains a tracking performance that closely resembles the optimal test without measurement noise interference. This result demonstrates that the emotional learning mechanism within the BELBIC-PID effectively suppresses the adverse effects of noisy feedback signals, which are unavoidable in practical sensing environments. The corresponding control efforts produced by all controllers are illustrated in Figure 25, with their enlarged views shown in Figure 26. As observed in Figure 26, the BELBIC-PID generates smoother control actions with minimal fluctuations, reflecting superior adaptability and robustness against measurement uncertainty.

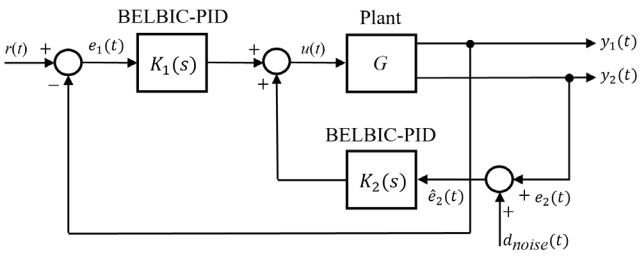

Figure 19. Deflection angle response of the FJM under measurement noise.

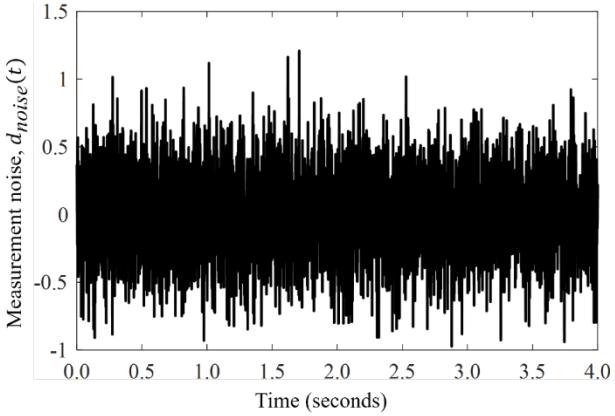

Figure 20. Measurement noise signal, $d_{noise}(t)$.

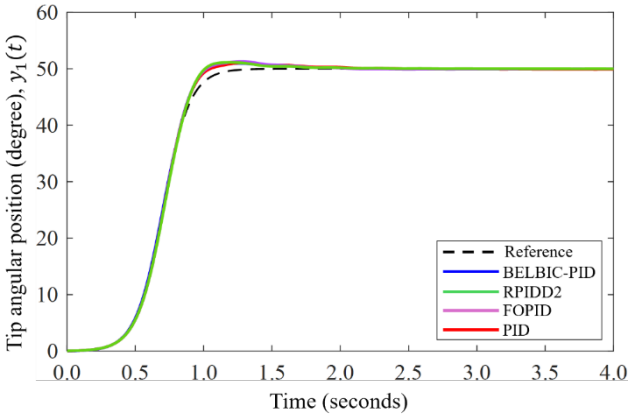

Figure 21. Tip angular position responses under measurement noise

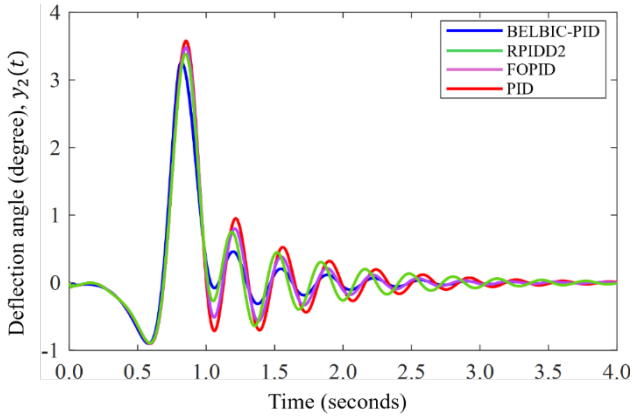

Figure 22. Deflection angle responses under measurement noise.

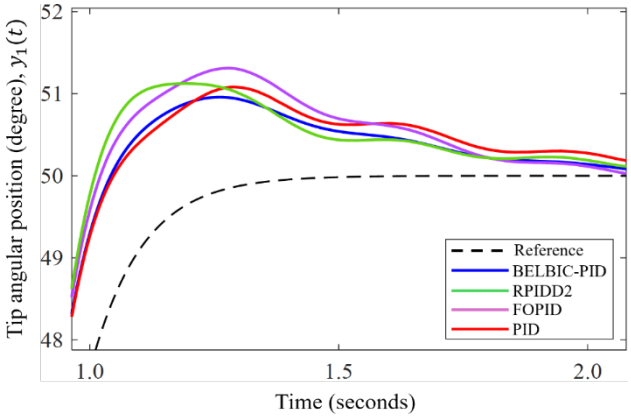

Figure 23. Zoomed view of the tip angular position responses under measurement noise.

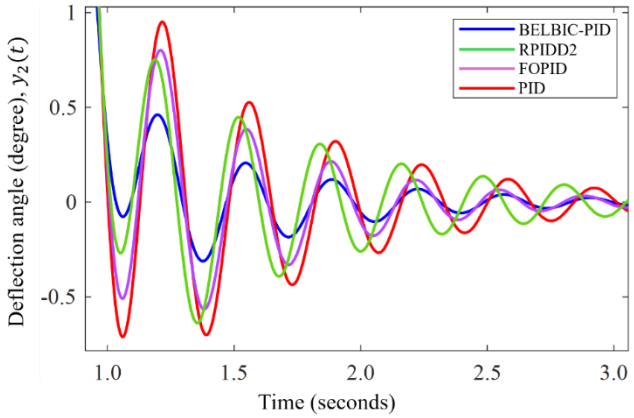

Figure 24. Zoomed view of the deflection angle responses under measurement noise.

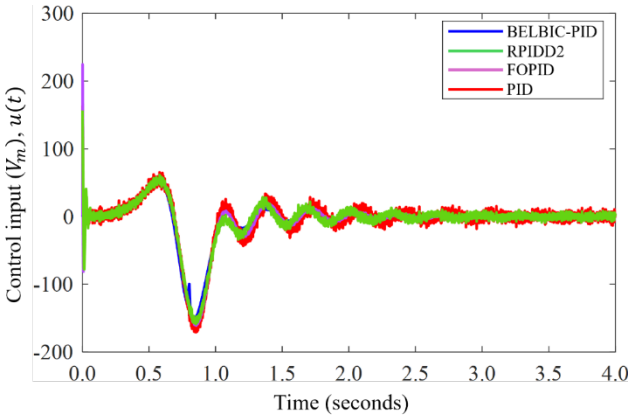

Figure 25. Control input responses under measurement noise.

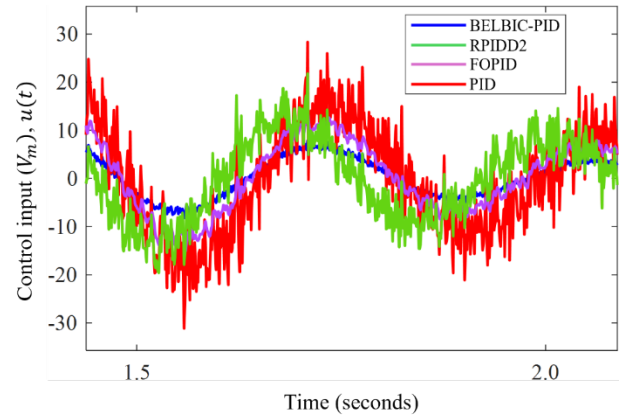

Figure 26. Zoomed view of the control input responses under measurement noise.

Moreover, Table 10 summarizes the performance indices of the BELBIC-PID and benchmark controllers under a noisy measurement environment. As shown, the BELBIC-PID consistently outperforms the benchmark controllers for both system outputs, demonstrating strong resilience to noisy feedback. For the tip angular position response $y_1(t)$, the proposed controller achieved the lowest values across all error-based indices, including ITSE, ITAE, ISE, and IAE, with respective reductions of 14.52%, 19.62%, 14.58%, and 19.46% relative to the PID controller. This improvement highlights the ability of the BELBIC-PID to preserve accurate tracking and favorable transient behavior even in the presence of measurement noise. For the deflection angle response $y_2(t)$, the BELBIC-PID also produced the smallest ITAE and IAE values of 0.9433 and 1.0241, corresponding to reductions of 37.55% and 25.11% compared with the PID controller, and consistently lower than those obtained with the FOPID and RPIDD2 controllers. The ITSE and ISE indices were similarly reduced by 26.56% and 20.79%, confirming the capability of the BELBIC-PID to suppress noise-induced fluctuations. Overall, these results affirm that the BELBIC-PID maintains superior tracking accuracy and robustness in noisy environments, attributed to its adaptive emotional learning mechanism that continuously adjusts the control signal in response to feedback variations.

Table 10. Trajectory tracking of the BELBIC-PID and benchmark controllers under measurement noise.

Responses measured	Performance indices	PID [40]	FOPID [43]	RPIDD2 [44]	BELBIC-PID
Tip angular position (degree), $y_1(t)$	ITSE	1.4092	1.8253	1.7169	**1.2046**
	ITAE	1.8554	1.7678	1.5909	**1.4913**
	ISE	1.2460	1.6445	1.6128	**1.0643**
	IAE	1.3954	1.4484	1.3742	**1.1239**
Deflection angle (degree), $y_2(t)$	ITSE	1.8852	1.6864	1.6320	**1.3844**
	ITAE	1.5106	1.2169	1.3737	**0.9433**
	ISE	2.1220	1.9529	1.8687	**1.6808**
	IAE	1.3675	1.2070	1.2504	**1.0241**

4. CONCLUSION

This work has proposed a data-driven BELBIC-PID controller for a FJM using MSEDA. The results show that the BELBIC-PID outperforms the conventional PID and its advanced variants in terms of control accuracy. In particular, the BELBIC-PID consistently achieved the lowest values of the fitness function and its associated performance indices. Its effectiveness was further validated by improved time-response characteristics for both system outputs. In addition, the controller produced the lowest values across all integral error indices, specifically ITSE, ITAE, ISE, and IAE, for both responses. These findings confirm that the nonlinear emotional learning mechanism of the BELBIC provides superior capability in handling the nonlinear characteristics of the FJM system. Furthermore, additional robustness evaluations under external disturbance and measurement noise conditions demonstrated that the BELBIC-PID maintains stable tracking performance and superior resilience compared with the benchmark controllers. Despite these promising results, the present study is limited to simulation-based validation and has not yet been implemented on a physical system. Future work will focus on experimental validation and the extension of this framework to other complex nonlinear MIMO systems to further verify its practical applicability. Moreover, this framework can be extended by redefining the external stimuli to the BELBIC through advanced PID controller variants to enhance its adaptability and learning efficiency. Overall, this work highlights the potential of the BELBIC-PID in improving control performance for nonlinear systems, where conventional PID and its advanced variants are often inadequate.

ACKNOWLEDGEMENT AND FUNDING

We thank the Ministry of Higher Education for funding this research through the Fundamental Research Grant Scheme (FRGS) No. FRGS/1/2024/TK07/UMP/03/1 (University reference RDU240101). We also sincerely thank Universiti Teknikal Malaysia Melaka and Universiti Malaysia Pahang Al-Sultan Abdullah for their invaluable support, which was instrumental in the successful completion of this study

DECLARATION OF CONFLICTING INTERESTS

The authors declare no potential conflicts of interest with respect to the research and publication of this article

REFERENCES

[1] S. Xu, Z. Wu and T. Shen, High-precision control of industrial robot manipulator based on extended flexible joint model, *Actuators*, 12, 2023, 1-17.

[2] H. Bilal, B. Yin, A. Kumar, M. Ali, J. Zhang and J. Yao, Jerk-bounded trajectory planning for rotary flexible joint manipulator: An experimental approach, *Soft Computing*, 27, 2023, 4029-4039.

[3] D.S. Carabis and J.T. Wen, Trajectory generation for flexible-joint space manipulators, *Frontier in Robotics and AI*, 9, 2022, 1-13.

[4] C. R. de Cos and J. Á. Acosta, Unified force and motion adaptive-integral control of flexible robot manipulators, *ISA Transactions*, 158, 2025, 586-593.

[5] M.J. Mahmoodabadi and N. Nejadkourki, Trajectory tracking of a flexible robot manipulator by a new optimized fuzzy adaptive sliding mode-based feedback linearization controller, *Journal of Robotics*, 2020, 1-12.

[6] S. Zaare, M.R. Soltanpour and M. Moattari, Adaptive sliding mode control of n flexible-joint robot manipulators in the presence of structured and unstructured uncertainties, *Multibody System Dynamics*, 47, 2019, 397-434.

[7] G. Rigatos and M. Abbaszadeh, Nonlinear optimal control for multi-DOF robotic manipulators with flexible joints, *Optimal Control Applications and Methods*, 42, 2021, 1708-1733.

[8] X. Cheng, H. Liu and W. Lu, Chattering-suppressed sliding mode control for flexible-joint robot manipulators, *Actuators*, 10, 2021, 1-24.

[9] R.F.A. Khan, K. Rsetam, Z. Cao and Z. Man, Singular perturbation-based adaptive integral sliding mode control for flexible joint robots, *IEEE Transactions on Industrial Electronics*, 70, 2023, 10516-10525.

[10] M.M. Arefi, N. Vafamand, B. Homayoun and M. Davoodi, Command filtered backstepping control of constrained flexible joint robotic manipulator, *IET Control Theory and Applications*, 17, 2023, 2506-2518.

[11] Y. Zhang, M. Zhang and F. Du, Robust finite-time command-filtered backstepping control for flexible-joint robots with only position measurements, *IEEE Transactions on Systems, Man, and Cybernetics: Systems*, 54(2), 2024, 1263-1275.

[12] R. Li, H. Wang, G. Yan, G. Li and L. Jian, Robust model predictive control for two-DOF flexible-joint manipulator system, *Mathematics*, 11(16), 2023, 1-25.

[13] H. Ma, Q. Zhou, H. Li and R. Lu, Adaptive prescribed performance control of a flexible-joint robotic manipulator with dynamic uncertainties, *IEEE Transactions on Cybernetics*, 52(12), 2022, 12905-12915.
[14] K. Kumar and R. Kumar, Boundary controllability of delay differential systems of fractional order with nonlocal condition, *Journal of Applied Nonlinear Dynamics*, 6, 2017, 465-472.
[15] Y. K. Ma, K. Kumar, R. Kumar, R. Patel, A. Shukla and V. Vijayakumar, Discussion on boundary controllability of nonlocal fractional neutral integrodifferential evolution systems, *AIMS Mathematics*, 7(5), 2022, 7642-7656.
[16] K. S. Chaudhary and N. Kumar, Hybrid neural network-based fractional-order sliding mode controller for tracking control problem of reconfigurable robot manipulators using fast terminal type switching law, *Engineering Applications of Artificial Intelligence*, 139, 2025, 1-15.
[17] B. K. Oleiwi, M. Jasim, A. T. Azar, S. Ahmed and A. R. Mahlous, Bat optimization of hybrid neural network-FOPID controllers for robust robot manipulator control, *Frontiers in Robotics and AI*, 12, 2025, 1-16.
[18] J. K. V and V. K. Elumalai, A proximal policy optimization based deep reinforcement learning framework for tracking control of a flexible robotic manipulator, *Results in Engineering*, 25, 2025, 1-15.
[19] T. Wang, Z. Ruan, Y. Wang and C. Chen, Control strategy of robotic manipulator based on multi-task reinforcement learning, *Complex & Intelligent Systems*, 11, 2025, 1-14.
[20] W. R. Abdul-Adheem, I. K. Ibraheem, A. J. Humaidi and A. T. Azar, Model-free active input–output feedback linearization of a single-link flexible joint manipulator: An improved active disturbance rejection control approach, *Measurement and Control*, 54(5-6), 2020, 856-871.
[21] H. V. Hultmann Ayala and L. Dos Santos Coelho, Tuning of PID controller based on a multiobjective genetic algorithm applied to a robotic manipulator, *Expert Systems with Applications*, 39(10), 2012, 8968-8974.
[22] J. Annisa, I. Z. Mat Darus, M. O. Tokhi and S. Mohamaddan, Implementation of PID based controller tuned by evolutionary algorithm for double link flexible robotic manipulator, *International Conference on Computational Approach in Smart Systems Design and Applications (ICASSDA)*, Kuching, Malaysia, 2018, 1-5.
[23] H. H. Baseri, H. Mohd Yatim, M. S. Hadi, M. H. Ab. Talib and I. Z. Mat Darus, Firefly algorithm for modeling of flexible manipulator system, *Recent Trends in Mechatronics Towards Industry 4.0*, Pekan, Malaysia, 2022, 235-251.
[24] A. Belkadi, H. Oulhadj, Y. Touati, S.A. Khan, B. Daachi, On the robust PID adaptive controller for exoskeletons: A particle swarm optimization based approach, *Applied Soft Computing*, 60, 2017, 87-100.
[25] L. Ramli, I. M. Lazim, A. A. Awi and A. S. Shukor, PID control and input shaping for quadrotor UAV stabilization and payload swing reduction, *Applications of Modelling and Simulation*, 9, 2025, 264-272.
[26] N. Živković, M. Lazarević and J. Vidaković, Fractional-order iterative learning control enhanced intelligent PID for articulated robots, *International Journal of Control, Automation and Systems*, 23, 2025, 2036-2045.
[27] K. Bin Gaufan, M. B. Aremu, N. M. Alyazidi and A. Nasir, Robust fractional-order sliding mode control for robotic manipulator system with time-varying disturbances, *Franklin Open*, 12, 2025, 1-10.
[28] Z. Zhang, B. Jiao, H. Sun, H. Lin and J. Shi, Collective and individual blade pitch control strategy for floating wind turbines based on improved ALO and fractional order PIDD2, *Ocean Engineering*, 341(4), 2025, 1-15.
[29] D. Izci, F.A. Hashim, S. Ekinci, S.F. Sabbeh, M. Bajaj, L. Prokop and I. Zaitsev, A novel cascaded RPIDD2-PI controller tuned by enhanced cooperation search algorithm for automatic voltage regulator systems, *IET Control Theory and Applications*, 19, 2025, 1-20.
[30] P. Sarkhel, N. Banerjee and N. B. Hui, Fuzzy logic-based tuning of PID controller to control flexible manipulators. *SN Applied Sciences*, 2(1124), 2020, 1-11.
[31] M. A. Ahmad, M. Z. M. Tumari and A. N. K. Nasir, Composite fuzzy logic control approach to a flexible joint manipulator, *International Journal of Advanced Robotic Systems*, 10(1), 2013, 1-9.
[32] C. Balkenius and J. Morén, Emotional learning: A computational model of the amygdala, *Cybernetics and Systems*, 32(6), 2001, 611-636.
[33] E. Lotfi and A. A. Rezaee, Generalized BELBIC, *Neural Computing and Applications*, 31, 2019, 4367-4383.
[34] C. Lucas, D. Shahmirzadi and N. Sheikholeslami, Introducing BELBIC: Brain emotional learning based intelligent controller, *Intelligent Automation and Soft Computing*, 10(1), 2004, 11-21.
[35] S. Saat, M. A. Ahmad and M. R. Ghazali, Data-driven brain emotional learning-based intelligent controller-PID control of MIMO systems based on a modified safe experimentation dynamics algorithm, *International Journal of Cognitive Computing in Engineering*, 6, 2025, 74-99.
[36] S. Saat, M. R. Ghazali, M. A. Ahmad, N. M. Z. A. Mustapha and M. Z. M. Tumari, An implementation of brain emotional learning based intelligent controller for AVR system, *International Conference on Automatic Control and Intelligent Systems (I2CACIS)*, Shah Alam, Malaysia, 2023, 60-64.
[37] J. Li, X. Luo, Y. Yuan and S. Gao, A nonlinear PID-incorporated adaptive stochastic gradient descent algorithm for latent factor analysis, *IEEE Transactions on Automation Science and Engineering*, 21(3), 2024, 3742-3756.
[38] J. De, J. Rubio, F. Gonzalez-Salazar and H. Calvo, Dynamic balance of a bipedal robot using neural network training with simulated annealing, *Frontiers in Neurorobotics*, 16, 2022, 1-16.
[39] C. Liang, F. Ripamonti, H. R. Karimi, S. Wrona and M. Pawełczyk, A stepwise simultaneous perturbation stochastic approximation algorithm for stability improvement of active noise control systems, *Mechanical Systems and Signal Processing*, 237, 2025, 1-14.
[40] M. A. Ahmad, H. Ishak, A. N. K. Nasir and N. A. Ghani, Data-based PID control of flexible joint robot using adaptive safe experimentation dynamics algorithm, *Bulletin of Electrical Engineering and Informatics*, 10(1), 2021, 79-85.
[41] M. Y. Silaa, O. Barambones and A. Bencherif, Robust adaptive sliding mode control using stochastic gradient descent for robot arm manipulator trajectory tracking, *Electronics*, 13(19), 2024, 1-20.

[42] J. Li, Y. Yuan, T. Ruan, J. Chen and X. Luo, A proportional-integral-derivative-incorporated stochastic gradient descent-based latent factor analysis model, *Neurocomputing*, 427, 2021, 29-39.
[43] A. Demirören, S. Ekinci, B. Hekimoğlu and D. Izci, Opposition-based artificial electric field algorithm and its application to FOPID controller design for unstable magnetic ball suspension system, *Engineering Science and Technology, an International Journal*, 24(2), 2021, 469-479.
[44] D. Izci and S. Ekinci, An improved RUN optimizer based real PID plus second-order derivative controller design as a novel method to enhance transient response and robustness of an automatic voltage regulator, *e-Prime - Advances in Electrical Engineering, Electronics and Energy*, 2, 2022, 1-11.
[45] M. S. O. Yeganeh, A. Oshnoei, N. Mijatovic, T. Dragicevic and F. Blaabjerg, Intelligent secondary control of islanded AC microgrids: A brain emotional learning-based approach, *IEEE Transactions on Industrial Electronics*, 70(7), 2023, 6711-6723.
[46] W. Fang, F. Chao, C.M. Lin, L. Yang, C. Shang and C. Zhou, An improved fuzzy brain emotional learning model network controller for humanoid robots, *Frontiers in Neurorobotics*, 13, 2019, 1-10.
[47] M. R. Khalghani, M. H. Khooban, E. Mahboubi-Moghaddam, N. Vafamand and M. Goodarzi, A self-tuning load frequency control strategy for microgrids: Human brain emotional learning, *International Journal of Electrical Power & Energy Systems*, 75, 2016, 311-319.
[48] M. Affan and R. Uddin, Brain emotional learning and adaptive model predictive controller for induction motor drive: A new cascaded vector control topology, *International Journal of Control, Automation and Systems*, 19, 2021, 3122-3135.
[49] M. U. Saeed, Z. Sun and S. Elias, Semi-active vibration control of building structure by self tuned brain emotional learning based intelligent controller, *Journal of Building Engineering*, 46, 2022, 1-24.
[50] J. R. Marden, H. P. Young, G. Arslan and J. S. Shamma, Payoff-based dynamics for multiplayer weakly acyclic games, *SIAM Journal on Control and Optimization*, 48(1), 2009, 373-396.